

# Scalable Experimental Bounds for Entangled Quantum State Fidelities

Shamminuj Aktar<sup>\*†‡</sup>, Andreas Bärtschi<sup>\*‡</sup>, Abdel-Hameed A. Badawy<sup>†</sup>, Stephan Eidenbenz<sup>‡</sup>

<sup>†</sup> Klipsch School of Electrical and Computer Engineering, New Mexico State University, Las Cruces, NM 88001, USA

<sup>‡</sup> CCS-3 Information Sciences, Los Alamos National Laboratory, Los Alamos, NM 87544, USA

<sup>\*</sup> Corresponding authors: [saktar@nmsu.edu](mailto:saktar@nmsu.edu), [baertschi@lanl.gov](mailto:baertschi@lanl.gov)

**Abstract**—Estimating the state preparation fidelity of highly entangled states on noisy intermediate-scale quantum (NISQ) devices is an important task for benchmarking and application considerations. Unfortunately, exact fidelity measurements quickly become prohibitively expensive, as they scale exponentially as  $O(3^N)$  for  $N$ -qubit states, using full state tomography with measurements in all Pauli bases combinations.

However, it is known [Somma et.al. 2006] that the complexity can be drastically reduced when looking at *fidelity lower bounds* for states that exhibit symmetries, such as Dicke States and GHZ States. For larger states, these bounds have so far not been tight enough to provide reasonable estimations on today's (2022) NISQ devices. In this work, for the first time and more than 15 years after the theoretical introduction, we report meaningful lower bounds for the state preparation fidelity of all Dicke States up to  $N = 10$  and all GHZ states up to  $N = 20$  on Quantinuum H1 ion-trap systems using efficient implementations of recently proposed scalable circuits for these states.

For example, we give state preparation fidelity lower bounds of (i) 0.46 for the Dicke State  $|D_3^{10}\rangle$  and (ii) 0.73 for the GHZ State  $|G_{20}\rangle$ . These match or exceed exact fidelity records recently achieved on superconducting systems for the much smaller states  $|D_3^6\rangle$  and  $|G_5\rangle$ , respectively. Furthermore, we provide evidence that for large Dicke States  $|D_{N/2}^N\rangle$ , we can resort to a GHZ-based approximate state preparation to achieve better fidelity.

**Index Terms**—Lower Bound, Fidelity, Entangled States, State Tomography, Quantinuum

## I. INTRODUCTION

Any advantage that quantum computing may have over classic computing usually relies on the principle of superposition, informally defined as being in multiple computational basis states at the same time. Quantum states that are in a superposition such that individual parts cannot be described independently of the state of others are called entangled states. Superposition and entanglement are essential prerequisites for the successful execution of additional gate operations per the overall structure of the quantum algorithm executed to ultimately lead to a desired quantum end state. Thus, proving that a NISQ device actually produces entangled states is a key necessary condition for any quantum computing success. Such low-level testing of quantum mechanical properties is necessary on quantum devices because environmental noise quickly modifies or partially destroys a pure quantum state (as it would be theoretically prepared); this noise process, usually

Research presented in this article was supported by the Laboratory Directed Research and Development program of Los Alamos National Laboratory under project number 20220656ER.

LA-UR-22-30105

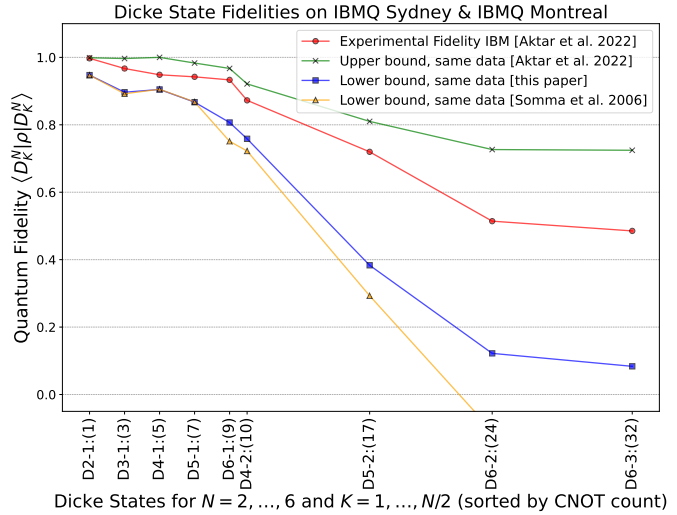


Fig. 1. Experimental fidelities of Dicke states  $|D_K^N\rangle$  (by circuit complexity) on IBMQ devices based on full state tomography data [2, Aktar et al.]: (red) Exact fidelity computed from all  $3^N$  tomography measurement settings, (green) Upper bound computed only from the  $Z$ -basis measurement data, (blue) We compute fidelity lower bounds from experimental  $X$ -,  $Y$ -, and  $Z$ -basis measurement setting subsets of their data, slightly improving on direct application of existing lower bound techniques [20, Somma et al.] (orange).

called decoherence, turns the actual state in a computing device into a so-called mixed state, which is a probabilistic mixture of our target pure quantum state and other pure states. The fidelity of a (mixed) quantum state measures to what extent the intended target (pure) quantum state has been realized; fidelity is defined to be 1 if we measure a correct pure quantum state, and it is close to zero, i.e.,  $1/2^n$  for a maximally mixed  $n$ -qubit quantum state that consist purely of noise.

Let us use the state  $\frac{1}{\sqrt{2}}(|00\rangle + |11\rangle)$ , i.e., the Bell state as the prototypical entangled state to illustrate the concept of fidelity. From a classical vantage point, it may appear tempting to test whether a NISQ device has actually produced a Bell state as follows: we execute a large number of runs of the generating circuit each with measurement at the end, and count how often we measure 00, 01, 10, and 11; if we measure 00 and 11 about 50 percent of the time each, we declare that the devices actually produces the Bell state. However, this logic is flawed because any classical device that simply returns

00 and 11 with probability 0.5 would have also passed our test, but such a cheat device would be useless and unable to properly execute additional gate operations that propagate the quantum state and its entanglement properly to execute any full quantum algorithm. The appropriate way to test entanglement is to calculate the fidelity measure (formally defined later), which measures the outcome in all possible combination bases of  $X$ ,  $Y$  and  $Z$  axes, thus requiring  $3^N$  tests for  $N$ -qubit states. This is usually called full state tomography. A fidelity measure of 1 indicates a perfect quantum state (with entanglement), where as a value of 0 indicates a state without entanglement.

Showing that entanglement exists on NISQ devices across more than 10 qubits is computationally prohibitive due to the exponential number of tests, but it nevertheless remains vital to demonstrate that the device actually leverages quantum mechanical principles.

A solution to this dilemma is to approximate or compute bounds on the fidelity measure that require fewer runs to calculate. [20] discovered such bounds for certain symmetric entangled states based on angular momentum operators. In this paper, we adopt and modify these generic bounds for the Dicke states, GHZ states, and approximate Dicke states – three well-known classes of entangled states; Dicke states are equal amplitude superpositions of all computational states of the same Hamming weight (i.e., number of ones) and GHZ states are Bell states that are generalized to larger qubit counts. We then show through a series of NISQ experiments that the bound from [20] has become useful in practice to provide evidence for entanglement across up to 20 qubits without resorting to exponentially expensive full state tomography. This is a testament to both advances in state preparation algorithms as well as as NISQ hardware improvements: we show that the original bounds are not useful for NISQ devices from just two years ago for Dicke states on as few as 5 qubits as they give negative values; they become slightly positive with our modifications without providing strong evidence of entanglement; however, newer technology (by Quantinuum) produces results good enough for these bounds to become meaningful lower bounds for the fidelity.

For example, we give state preparation fidelity lower bounds of (i) 0.46 for the 10-qubit Dicke State  $|D_5^{10}\rangle$  and (ii) 0.73 for the 20-qubit GHZ State  $|G_{20}\rangle$ . These match or exceed exact fidelity records recently achieved on superconducting systems for the much smaller states  $|D_3^6\rangle$  and  $|G_5\rangle$ , respectively.

The original as well as our modified fidelity bounds require only three different measurement runs, thus making fidelity based entanglement verification easily accessible on NISQ devices even at high qubit counts.

## II. RELATED WORK

We use the *quantum fidelity*  $\mathcal{F}$  as a similarity measure between a prepared mixed state  $\rho$ , expressed as a density matrix, and a target pure quantum state  $\rho_\psi = |\psi\rangle\langle\psi|$  [13]:

$$\mathcal{F}(\rho_\psi, \rho) = \left[ \text{Tr} \sqrt{\sqrt{\rho} \rho_\psi \sqrt{\rho}} \right]^2 = \text{Tr}(\rho_\psi \rho) = \langle \psi | \rho | \psi \rangle \quad (1)$$

where  $\sqrt{\rho}$  denotes the unique positive semi-definite square root of  $\rho$  such that  $\sqrt{\rho} \sqrt{\rho} = \sqrt{\rho}^\dagger \sqrt{\rho} = \rho$ , and where the first equality would also hold for a mixed state  $\rho_\psi$ . In this paper, we consider pure target states, notably Dicke states  $|D_K^N\rangle$  and GHZ states  $|G_N\rangle$ . We remark that quantum fidelity is sometimes also defined as  $\mathcal{F}' = \sqrt{\mathcal{F}}$  [18], [20]. In a straightforward way, the fidelity of a prepared  $N$ -qubit state can be computed by sampling  $\rho$  in  $3^N$  different Pauli basis ( $N$ -fold tensor products of Pauli operators  $\sigma_x, \sigma_y$  and  $\sigma_z$ ) to reconstruct its density matrix, from which we can compute the fidelity with the target state.

If one wants to *upper bound* the quantum fidelity, then one can consider the *measurement success probability*, i.e. the overall probability of sampling non-zero amplitude states when measuring in the computational  $Z$ -basis:

$$MSP(\rho_\psi, \rho) := \sum_{x \in \{0,1\}^n, \langle x | \rho_\psi | x \rangle \neq 0} \langle x | \rho | x \rangle \quad (2)$$

Using a double application of the Cauchy-Schwarz inequality, one gets  $\mathcal{F}(\rho_\psi, \rho) \leq MSP(\rho_\psi, \rho)$  [2].

Several works have shown that it is possible to estimate a *lower bound* on the quantum fidelity using only few measurement settings avoiding the full state tomography. Earlier works [11], [20] focused on special states that have unique symmetry which require only a small random subset of Pauli operators to estimate fidelity. Somma et al. [20] proposed expressions for estimating quantum fidelity for highly symmetric classes of multi-qubit state preparation i.e. rotational invariant states, stabilizer states and generalized coherent states. To estimate lower bound of fidelity, they only used the measurements that have relation with the symmetry operators of the density matrix. Also, [11] derived fidelity estimation for GHZ and  $W$  states using  $2N - 1$  measurements. A generalized approach by Flammia et al. [9] showed estimation techniques for all possible state preparation by measuring lesser number of Pauli operators that are close to the desired state and of greater importance. Mentioning the scalability issue in generalized  $N$  qubit state fidelity estimation, Elben et al. [8] showed how randomized measurement can enable fidelity estimation by comparing two states. Recently, Zhang et al. [25] proposed machine learning based approach for direct fidelity estimation as a classification problem using a constant number of expectations.

Additionally, quantum state verification (also known as non-tomographic method) uses advanced statistical approaches to verify whether the output of some device is the target state. Previous works on quantum state verification techniques validates specific state preparation such as Dicke states [16], GHZ states [15], Hypergraph states [26], Pure states [14], [22], [23], [27] etc. There are also some generalized approaches for state verification [12], [19], [24], [28], [29] and [21].

## III. FIDELITY LOWER BOUNDS FOR DicKE STATES

We provide experimental lower bound estimations on the state preparation fidelity of Dicke states  $|D_K^N\rangle$  (up to  $N = 10$ ). We first discuss the circuit preparation strategies, then provide

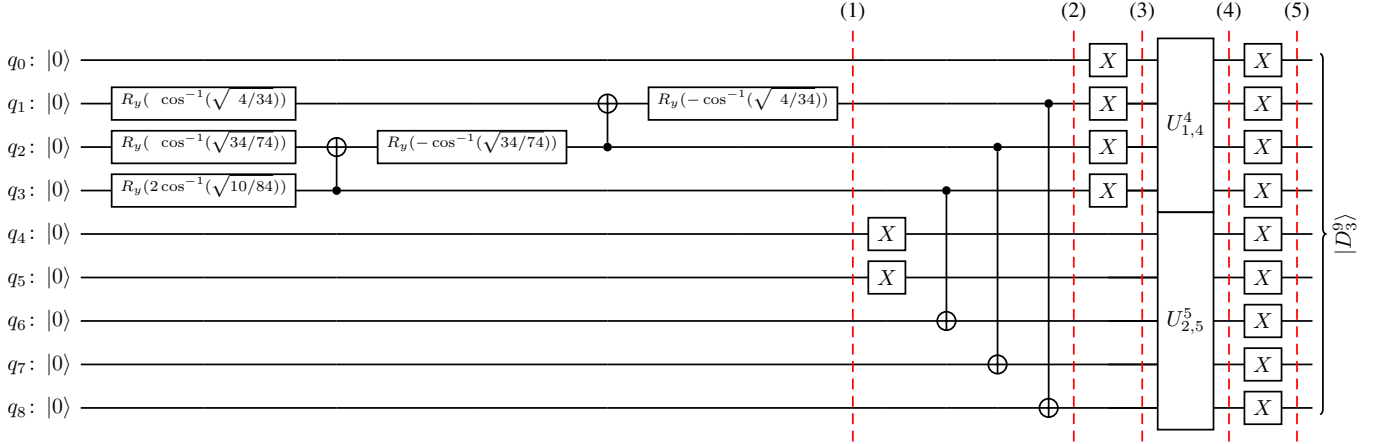


Fig. 2. Preparation of the Dicke state  $|D_3^9\rangle$  with a divide-and-conquer approach allowing parallelizable Dicke state unitaries on 4 and 5 qubits, respectively: (1) We first prepare a correctly weighted superposition of input Hamming weights  $0 \leq \ell \leq 3$  on the first register. The used  $R_y$ -rotations contain arguments with numerators (denominators) derived from (suffix-sums) of terms of the form  $\binom{5}{3-\ell} \binom{4}{\ell}$ , the number of distributions of  $\ell$  &  $3-\ell$  Ones across 4 & 5 qubits. (2&3) The first register is correctly entangled with the second register, and bit-flipping  $X$ -gates are applied to reduce the number of CNOTs in the following. (4&5) Parallel Dicke state unitaries  $U_{1,4}^4$  and  $U_{2,5}^5$  prepare the Dicke state  $|D_6^9\rangle$ , followed by bit-flipping  $X$ -gates to get  $|D_3^9\rangle$ .

lower bound expressions for estimating quantum fidelity and present experimental result for fidelity estimation in Quantinuum's H1-2 quantum processor.

#### A. State Preparation

A Dicke state  $|D_K^N\rangle$  is the equal weight superposition of all  $\binom{N}{K}$   $N$ -qubit basis states  $x$  with  $K$  Ones and  $N-K$  Zeroes, i.e., with Hamming weight  $\text{wt}(x) = K$ :

$$|D_K^N\rangle = \binom{N}{K}^{-1/2} \sum_{x \in \{0,1\}^N, \text{wt}(x)=K} |x\rangle. \quad (3)$$

We optimize and generalize existing work on Dicke state preparation by defining Dicke state unitaries  $U_{k,K}^N$  which prepare Dicke states  $|D_\ell^N\rangle$  upon any input of a unary encoded Hamming weight  $k \leq \ell \leq K$ :

$$U_{k,K}^N: |0^{N-\ell} 1^\ell\rangle \mapsto |D_\ell^N\rangle \quad \forall k \leq \ell \leq K. \quad (4)$$

Dicke state unitaries were first defined for  $k := 0$  [3], and there exists a linear-depth circuit construction for  $k := 0$ ,  $K := N$  with  $5\binom{N-1}{2} + 2(N-1)$  two-qubit CNOT gates between neighboring qubits in a 1D Linear Nearest Neighbor (LNN) connectivity only [2]. We start from this construction and further reduce the CNOT count by  $3\binom{N-K-1}{2}$  and  $5\binom{k}{2}$  using ideas for upper [3] and lower [17] bounds on the Hamming weight  $\ell$ , respectively. This effectively generalizes and also improves all of the former constructions by constant factors while preserving LNN connectivity.

To prepare a fixed- $K$  Dicke state  $|D_K^N\rangle$ , we further parallelize our construction using a divide-and-conquer strategy [2], [4]: The main idea is to split the Hamming weight  $K$  across qubit sets of size  $N_1 = \lfloor \frac{N}{2} \rfloor$  and  $N_2 = \lceil \frac{N}{2} \rceil$  using  $2K-1$  CNOT gates on an all-to-all connectivity before applying the Dicke state unitaries  $U_{0,K}^{N_1}$  and  $U_{0,K}^{N_2}$  in parallel. Additional gains can be made by implementing these unitaries with layers of bit-flipping Pauli- $X$  gates,  $U_{0,K}^{N_i} = X^{\otimes N_i} \cdot U_{N_i-K, N_i}^{N_i}$ .

$X^{\otimes N_i}$ , resulting in the circuit structure shown in Figure 2, which prepares  $|D_3^9\rangle$  with the following steps:

$$\begin{aligned} |0^5\rangle |0^4\rangle &\xrightarrow{(1)} \binom{9}{3}^{-1/2} \sum_{\ell=0}^3 \sqrt{\binom{5}{3-\ell} \binom{4}{\ell}} |00000\rangle |1^\ell 0^{3-\ell} 0\rangle \\ &\xrightarrow{(2)} \binom{9}{3}^{-1/2} \sum \sqrt{\binom{5}{3-\ell} \binom{4}{\ell}} |0^{3-\ell} 1^\ell 11\rangle |1^\ell 0^{3-\ell} 0\rangle \\ &\xrightarrow{(3)} \binom{9}{3}^{-1/2} \sum \sqrt{\binom{5}{3-\ell} \binom{4}{\ell}} |0^{3-\ell} 1^\ell 11\rangle |0^\ell 1^{3-\ell} 1\rangle \\ &\xrightarrow{(4)} \binom{9}{3}^{-1/2} \sum \sqrt{\binom{5}{3-\ell} \binom{4}{\ell}} |D_{2+\ell}^5\rangle |D_{4-\ell}^4\rangle \\ &\xrightarrow{(5)} \binom{9}{3}^{-1/2} \sum \sqrt{\binom{5}{3-\ell} \binom{4}{\ell}} |D_{3-\ell}^5\rangle |D_\ell^4\rangle = |D_3^9\rangle. \end{aligned}$$

Note that to prepare the Dicke state  $|D_6^9\rangle$  we can simply omit the last layer of Pauli- $X$  gates. Thus in our experiments we only prepare Dicke states  $|D_K^N\rangle$  up to  $K \leq \frac{N}{2}$ , for which our two-qubit gates amount to  $5K(N-K) - 3(N+K) + 5$  CNOTs, giving linear depth  $\mathcal{O}(N)$  and total gate count  $\mathcal{O}(KN)$ .

#### B. Lower bounds for fidelity estimation

Following [20], we observe that Dicke States are rotationally invariant and thus are the unique simultaneous eigenstates of the (squared) total angular momentum  $J^2 = J_x^2 + J_y^2 + J_z^2$  and its  $z$ -component  $J_z$ , where  $J_\tau = \sigma_\tau^1 + \sigma_\tau^2 + \dots + \sigma_\tau^N$  for Pauli operators  $\sigma_\tau^i$ ,  $\tau = x, y, z$ , acting on qubit  $i$ . This means we can write the Dicke state  $|D_K^N\rangle$  as  $|j, j_z\rangle$  in terms of its quantum numbers  $j = N$  and  $j_z = N - 2K$  with:

$$J^2 |j, j_z\rangle = j(j+2) |j, j_z\rangle \quad (5)$$

$$J_z |j, j_z\rangle = j_z |j, j_z\rangle. \quad (6)$$

In general, the quantum numbers  $j$  and  $j_z$  satisfy  $0 \leq j \leq N$  and  $|j_z| \leq j$  and the difference between any two eigenvalues is at least 2 (because we use Pauli operators instead of spin-1/2 operators).

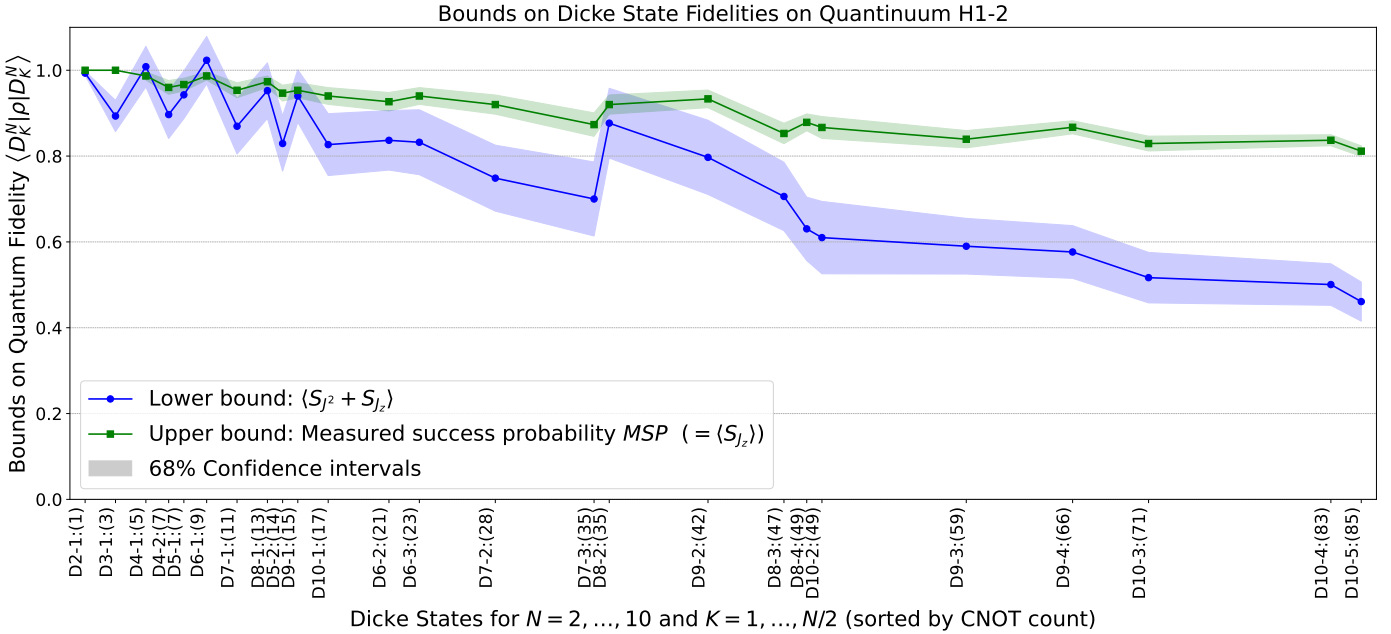


Fig. 3. Upper and lower bounds on the quantum fidelity  $\langle D_K^N | \rho | D_K^N \rangle$  for Dicke States  $|D_K^N\rangle$  on Quantinuum H1-2, including 68% confidence intervals. Dicke states are sorted along the  $x$ -axis according to the number of CNOTs in their preparation circuits. The bump in fidelity for Dicke states  $|D_1^8\rangle$ – $|D_4^8\rangle$  and  $|D_1^9\rangle$ – $|D_2^9\rangle$  may be due to these experiments taking place right after a recalibration downtime of the QPU.

Now we can write a target state  $\rho_{j,j_z} := |j, j_z\rangle \langle j, j_z|$  in terms of the operators  $J^2$  and  $J_z$ :

$$\rho_{j,j_z} = \prod_{\substack{j'_z \neq j_z \\ -j \leq j'_z \leq j}} \frac{J_z - j'_z}{j_z - j'_z} \prod_{0 \leq j' \leq N} \frac{J^2 - j'(j' + 2)}{j(j + 2) - j'(j' + 2)}. \quad (7)$$

We could compute the fidelity  $\mathcal{F}(\rho_{j,j_z}, \rho)$  by measuring every Pauli-String that appears when we expand the product, i.e., all correlations between the operators  $J^2$  and  $J_z$  in in Equation (7). This process still requires measurement of an exponentially large number of observables but less than  $3^N$  measurements of performing full state tomography.

Instead we turn towards the construction of operators that allow us to compute a lower bound on the fidelity. We will define operators  $\mathcal{S}_{J_z}$  and  $\mathcal{S}_{J^2}$  inspired by the density operator of Equation (7) such that they satisfy  $[\mathcal{S}_{J_z} + \mathcal{S}_{J^2}] |j', j'_z\rangle = e_{j', j'_z} |j', j'_z\rangle$  with  $e_{j', j'_z} = 1$  for the correct Dicke state and  $e_{j', j'_z} \leq 0$  for  $(j', j'_z) \neq (j, j_z)$ . We define the operator  $\mathcal{S}_{J_z}$  as the left-hand product in Equation (7),

$$\mathcal{S}_{J_z} := \prod_{j'_z \neq j_z} [(J_z - j'_z)/(j_z - j'_z)], \quad (8)$$

for which  $|j', j'_z\rangle$  has eigenvalue 1 if  $j'_z = j_z$  and 0 otherwise.<sup>1</sup> Expanding the product results in Pauli-Strings consisting of identities and  $\sigma_z$  operators only. These commute pairwise, hence we can measure  $\mathcal{S}_{J_z}$  in the computational basis and thus in a single measurement setting. In fact, we get the measurement success probability  $\text{Tr}[\mathcal{S}_{J_z}, \rho] = \text{MSP}(\rho_{j,j_z}, \rho)$ .

<sup>1</sup>We note that in [20], the operator is defined as  $\mathcal{S}_{J_z} = -\frac{1}{4}(J_z - j_z)^2 + 1$ , which for states  $|j', j'_z \neq j_z\rangle$  leads to eigenvalues  $\leq 0$  instead of a strict equality =0. This results in less tight bounds, see Figure 1.

The same is not true if we expanded the right-hand product of Equation (7): we would get a large number of non-commuting Pauli-Strings. Instead we use the following definition for  $\mathcal{S}_{J^2}$  [20], which is based on the observation that Dicke states have maximum angular momentum, and all other eigenvalues for  $J^2$  deviate by at least  $N(N+2) - (N-2)N = 4N$ :

$$\mathcal{S}_{J^2} = \frac{1}{4N}(J^2 - N(N+2)), \quad (9)$$

for which  $|j', j'_z\rangle$  has eigenvalue 1 if  $j' = j = N$  and integer eigenvalues  $\leq 0$  otherwise. Similar to  $\mathcal{S}_{J_z}$ , we can measure the operator  $\mathcal{S}_{J^2}$  by computing  $\text{Tr}(J_\tau^2, \rho)$  through measurement in the  $\tau$ -basis, i.e., measuring in the three  $X$ -basis,  $Y$ -basis and  $Z$ -basis settings is enough.

If the sum of the operators  $\mathcal{S}_{J_z}$  and  $\mathcal{S}_{J^2}$  are applied to a target Dicke state  $\rho = |j', j'_z\rangle$ , we get eigenvalue 1 for the correct Dicke state and eigenvalues  $\leq 0$  for all other rotational states. In general, if  $|\phi\rangle = \sum_{j', j'_z} c_{j', j'_z} |j', j'_z\rangle$  is a pure state, then we get

$$\langle \phi | \mathcal{S}_{J_z} + \mathcal{S}_{J^2} | \phi \rangle = \sum_{j', j'_z} (e_{j', j'_z}) |c_{j', j'_z}|^2 \quad (10)$$

Here  $|c_{j,j_z}|^2$  is the probability of projecting  $|\phi\rangle$  onto the state  $|j = N, j_z = N - 2K\rangle$ . Our experimentally prepared mixed state  $\rho$  is a convex combination of pure states, yielding our lower bound

$$\langle \mathcal{S}_{J_z} + \mathcal{S}_{J^2} \rangle := \text{Tr}[\mathcal{S}_{J_z} + \mathcal{S}_{J^2}, \rho] \leq \mathcal{F}(\rho_{j,j_z}, \rho) \quad (11)$$

### C. Experimental Result

We construct Dicke state  $|D_K^N\rangle$  circuits using the preparation scheme described in Section III-A. We use IBM Qiskit [1]

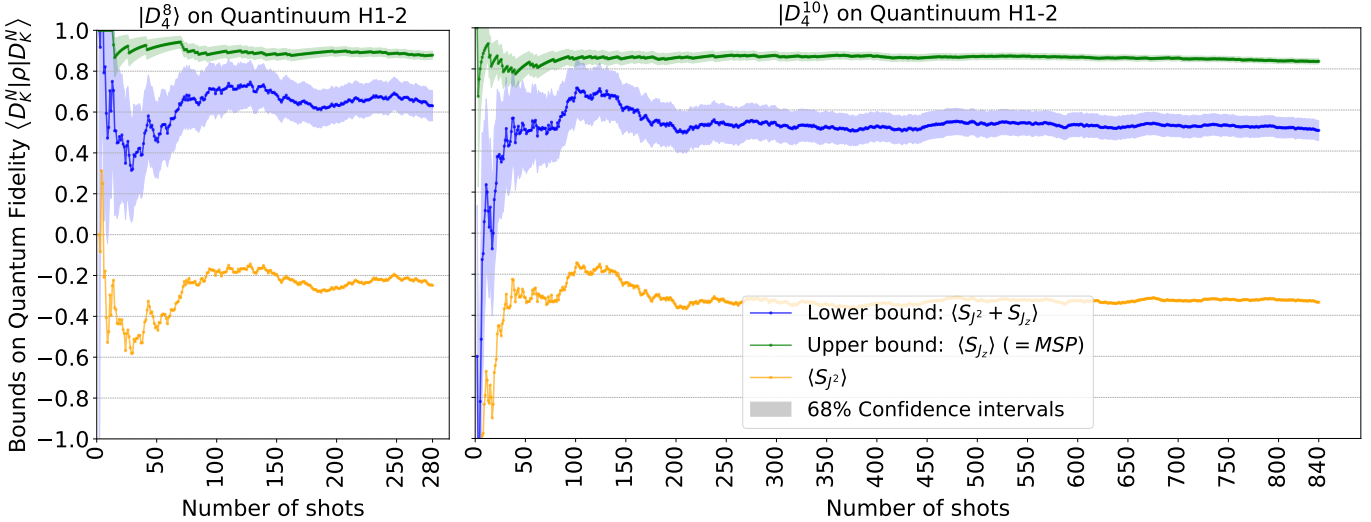


Fig. 4. Evolving bounds and confidence intervals on Dicke state fidelity  $\langle D_K^N | \rho | D_K^N \rangle$  for  $|D_4^8\rangle$  and  $|D_4^{10}\rangle$  on Quantinuum H1-2 with increasing shot count. Experiments were run for 280 and 840 shots for  $|D_4^8\rangle$  and  $|D_4^{10}\rangle$ , respectively, to achieve comparable confidence intervals. Plots are scaled (1:3) accordingly.

to prepare the circuits and we did not apply the Qiskit transpilation and optimization options. To obtain the bounds on fidelity, first we generate the untranspiled QASM circuits for Dicke State  $|D_K^N\rangle$  where  $2 \leq N \leq 10$  and  $1 \leq K \leq N/2$ . Next, we compute the bounds on the quantum fidelity using only three measurements ( $X$ ,  $Y$  and  $Z$  basis measurement) instead of measuring  $3^N$  state tomography circuits to measure the closeness of prepared Dicke state  $\rho$  to the expected Dicke state  $|D_K^N\rangle$ . We use the formulas of Section III-B to estimate the lower bound  $\langle S_{J_z} + S_{J^2} \rangle_\rho$  on quantum fidelity  $\langle D_K^N | \rho | D_K^N \rangle$ . We also show the probability of finding expected basis states among a total number of circuit executions (informally called measured success probability). The definition of  $S_{J_z}$  in 8 shows that it is the measured success probability of the prepared Dicke state.

1) *Overall Result:* Figure 3 shows the bounds for Dicke State  $|D_K^N\rangle$  where  $N = 2$  to  $10$  and  $K = 1$  to  $N/2$ . The Dicke states from left to right are sorted according to the number of required CNOT gates in the untranspiled circuit. In  $X$  axis, Dicke states  $|D_K^N\rangle$  are represented as  $D - N - K : (C)$  where  $N$  is number qubits,  $K$  is hamming weight and  $C$  is number of CNOT counts. The plot shows the lower bound  $\langle S_{J_z} + S_{J^2} \rangle_\rho$  and measurement success probability along with two-sided 68% confidence interval below and above the mean of the distribution. We observe statistical noise in the lower bound estimation for the smaller Dicke states (with few CNOTs). We also find that the fidelity lower bound decreases with the increasing number of CNOT gates on both simulator and real hardware. We also observe that the lower bound estimation of Dicke states is better in hardware than the ones in the simulator. For our largest Dicke state  $|D_5^{10}\rangle$ , the simulator lower bound estimation on fidelity is 0.22 while the hardware estimation is 0.46. Quantinuum specification mentions that although the simulators provide a high fidelity representation of the hardware device's output, some variances between the

results may occur as the noise models in the simulator cannot fully capture the real hardware behavior. This explains the difference between simulator and hardware estimations of lower bounds on quantum fidelities. The sudden inconsistency of lower bound estimation from  $|D_2^8\rangle$  could be because the experiments before and after  $|D_2^8\rangle$  were executed in a different time span. Moreover, the experiments after  $|D_3^7\rangle$  were run just after the H1-2 machine became online after calibration. The plot also shows that the measured success probability represents the upper bound of quantum fidelity and the gap between lower bound & upper bound starts to increase for higher Dicke states.

2) *Number of Shots:* We ran the Dicke state circuits on Quantinuum H1-2E simulator using  $\max(150, 4 * \text{num\_states})$  shots where  $\text{num\_states} = {}^N C_K$  for  $N = 2$  to 10 and  $K = 1$  to  $N/2$ . Figure 4 shows cumulative measurements of bounds on quantum fidelity  $\langle D_K^N | \rho | D_K^N \rangle$ . The left plot shows bounds on quantum fidelity for Dicke state  $|D_4^8\rangle$  & the right plot shows the bounds for Dicke state  $|D_4^{10}\rangle$  on H1-2 quantum device. In each plot, the  $X$ -axis shows the number of shots and  $Y$ -axis shows the cumulative bound estimations. Each plot shows three cumulative lines: lower bound  $\langle S_{J_z} + S_{J^2} \rangle$ , upper bound measured success probability and  $S_{J^2}$ . The plots also show two-sided 68% confidence interval below mean and above mean for lower bound and measured success probability  $S_{J_z}$ . The plots are scaled according to the maximum number of shots used in the execution of the circuit. In each plot, we find that initially there are a lot of fluctuation in the lower bound and upper bound estimation but the estimations start to get balanced with the increasing number of shots. Similarly, the confidence interval region follows the lower bound estimation and shows how the estimation starts to be stable at the end. The cumulative measurement success probability of the experiments represents the upper bound of quantum fidelity which stabilizes faster

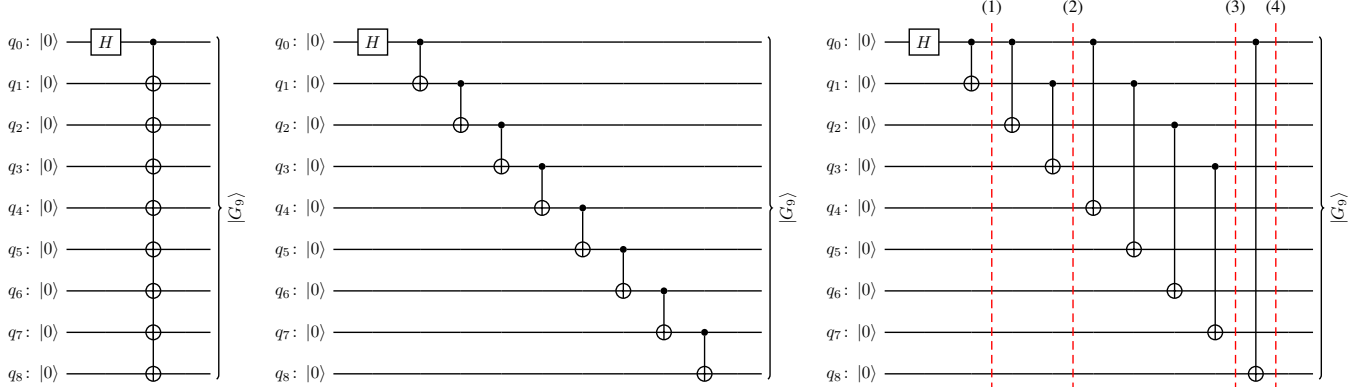


Fig. 5. Preparation of a ( $N = 9$ )-qubit GHZ state  $|G_9\rangle$ : (left) Schematics, (center) Linear-depth circuit on LNN connectivity, (right) Logarithmic-depth circuit on full connectivity. For the linear depth GHZ circuit all CNOT gates are executed consecutively and generate a linear time  $O(N)$  complexity. For the logarithmic depth GHZ circuit the gates leading to (1),(2),(3) & (4), respectively, can be executed in parallel and generate a logarithmic  $O(\log N)$  complexity.

than the lower bounds.

#### IV. FIDELITY LOWER BOUNDS FOR GHZ STATES

We provide experimental lower bound estimations on quantum fidelity for GHZ states  $|G_N\rangle$  (upto  $N = 20$ ). First, we discuss the circuit preparation strategies, then we provide lower bound expressions for estimating quantum fidelity in state preparation and finally present experimental result for fidelity estimation in Quantinuum's H1-1 quantum processor.

##### A. State Preparation

An  $N$ -qubit GHZ state is equal weight superposition of all zeros and all one's defined as

$$|G_N\rangle = \frac{|0\rangle^{\otimes N} + |1\rangle^{\otimes N}}{\sqrt{2}}. \quad (12)$$

The straightforward way to prepare  $|G_N\rangle$  is first initializing all qubits to  $|0\rangle^{\otimes N}$ . The next step is adding a Hadamard gate  $H$  to the first qubit and then consecutively adding CNOT gate between  $i^{th}$  and  $(i+1)^{th}$  qubit where  $i = 0$  to  $N-1$ . This circuit generates a linear time complexity of  $N$ . Recent work showed that some CNOT gates can be rearranged in GHZ state preparation without affecting the output state that will allow execution of the CNOT gates in parallel [7]. Such rearrangement reduces the execution step of the GHZ circuit and generates logarithmic depth GHZ circuits with time complexity  $1 + \log_2 N$ . Figure 5 shows  $N = 10$  qubit linear (left) and logarithmic depth (right) GHZ state preparation from initial state  $|0\rangle^{\otimes N}$ . Both circuits contain  $N$  gates (1 Hadamard and  $(N-1)$  CNOTs). The dotted lines in the right plot indicate slices within which the CNOT gates can be performed in parallel. The linear depth circuit (left) requires serial execution of the CNOT gates after the first Hadamard gate that induces linear time complexity of  $N = 10$ . In the logarithmic depth  $|G_N\rangle$  circuit, the CNOT gates in each time slice executes in parallel that generates logarithmic complexity of  $1 + \log_2 N = 1 + \log_2(10) \approx 4$ .

##### B. Lower bounds for fidelity estimation

GHZ states lies in the family of stabilizer states that are used in quantum error correction procedures. From [20], we find that stabilizer states can be defined by symmetry operators,

$$\hat{O}_s = +1 |\psi\rangle ; s \in [1, S] \quad (13)$$

Here the stabilizer operator  $\hat{O}_s$  are products of Pauli operators that take +1 or -1 as possible eigen values. A stabilizer state  $|\psi\rangle$  can be uniquely defined by 13 where  $G_s = \{\hat{O}_1, \dots, \hat{O}_s\}$  forms the stabilizer group.  $G_s$  can also be defined using its  $L$  linear independent generators [10],  $G_s \equiv (\hat{g}_1, \dots, \hat{g}_L)$  where

$$\hat{g}_i |\psi\rangle = +1 |\psi\rangle , i \in [1, L] \quad (14)$$

Thus, the state  $|\psi\rangle$  can be expressed as  $|\psi\rangle = |g_1 = 1, \dots, g_L = 1\rangle$  while the density operator  $\rho_\psi$  can be defined as

$$\begin{aligned} \rho_\psi &= |g_1 = 1, \dots, g_L = 1\rangle \langle g_1 = 1, \dots, g_L = 1| \\ &= \frac{1}{2^L} \prod_{i=1}^L (\hat{g}_i + \mathbb{1}) \end{aligned} \quad (15)$$

The fidelity of a prepared state  $|\rho\rangle$  can be measured by computing the expectations listed in 15. From [20], we find that a lower bound on the fidelity can be estimated using the operator  $\mathcal{S}_{G_s} = \frac{1}{2}[(\sum_{i=1}^L \hat{g}_i) - (L-2)]$ . When the operator  $\mathcal{S}_{G_s}$  is applied to the state  $|\psi\rangle = |g_1, \dots, g_L\rangle$ , we get,

$$\mathcal{S}_{G_s} |g_1, \dots, g_L\rangle = e_{g_1, \dots, g_L} |g_1, \dots, g_L\rangle , (g_i = \pm 1) \quad (16)$$

where  $e_{1, \dots, 1} = 1$  and  $e_{g_1, \dots, g_L} \leq 0$ . The lower bound on fidelity between prepared state  $\rho$  and expected state  $|G_N\rangle$  becomes

$$\mathcal{F}(|G_N\rangle, \rho) \geq \langle \mathcal{S}_{G_s} \rangle_\rho \quad (17)$$

Using the formulas above for an  $N$ -qubit GHZ state  $|G_N\rangle$ , the stabilizer group can be defined as  $G_s \equiv (\sigma_x^1 \sigma_x^2 \dots \sigma_x^N, \sigma_z^1 \sigma_z^2 \dots \sigma_z^N)$ . We can estimate the

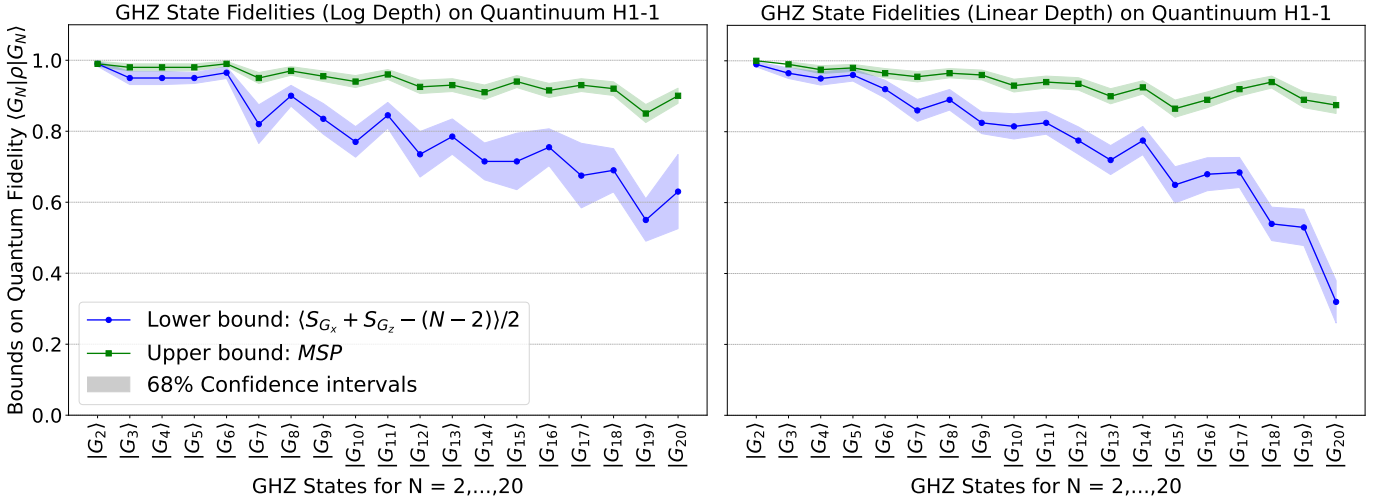


Fig. 6. Upper and lower bounds on quantum fidelity  $\langle G_N | \rho | G_N \rangle$  for GHZ States  $|G_N\rangle$  on Quantinuum H1-1 up to  $N = 20$ , including 68% confidence intervals. The left plot shows results for logarithmic depth state preparation circuits, while the right plot shows results for a linear depth state preparation.

lower bounds on GHZ state fidelities using only the Pauli  $X$  and Pauli  $Z$  measurement and  $\mathcal{S}_{G_s}$  will be defined as

$$\mathcal{S}_{G_s} = \frac{1}{2} [\mathcal{S}_{G_x} + \mathcal{S}_{G_z} - (N - 2)] \quad (18)$$

where  $\mathcal{S}_{G_x}$  represents product of Pauli  $X$  operator on  $i = 1$  to  $N$  qubits and  $\mathcal{S}_{G_z}$  represents sum of the pairwise products of Pauli  $Z$  operator on  $i^{th}$  and  $(i+1)^{th}$  qubit upto  $N^{th}$  qubit. For a 4-qubit GHZ state, we get  $N = 4$  and  $L = 4$ ,

$$\mathcal{S}_{G_s} = \frac{1}{2} [\sigma_x^1 \sigma_x^2 \sigma_x^3 \sigma_x^4 + \sigma_z^1 \sigma_z^2 + \sigma_z^2 \sigma_z^3 + \sigma_z^3 \sigma_z^4 - 2]. \quad (19)$$

Basically we need to compute the expectation of the product of Pauli  $X$  measurement on each of the four qubit by taking  $+1$  for even parity and  $-1$  for odd parity. Similarly, we compute pairwise consecutive product of Pauli  $Z$  measurement on qubit 1 & 2, 2 & 3 and 3 & 4 by checking the pairwise parity. Then we get an estimation of the fidelity lower bound for GHZ state by taking the average of those products and subtracting  $N - 2$  from the sum.

### C. Experimental Result

We prepare linear depth and logarithmic depth GHZ states  $|G_N\rangle$  circuits mentioned in Section IV-A. Similar to the Dicke state circuits, we use IBM Qiskit [1] to construct the circuits with no compilation and optimizations. In this experiment, we generate untranspiled QASM circuits for GHZ states  $|G_N\rangle$ , where  $2 \leq N \leq 20$ . We compute the bounds on quantum fidelity using only two measurements ( $X$  and  $Z$  basis measurement) instead of measuring  $3^N$  state tomography circuits to measure the closeness of prepared GHZ state  $\rho$  to the expected state  $|G_N\rangle$ . To estimate lower bound  $\langle \mathcal{S}_{G_s} \rangle_\rho$ , we followed the idea described in Section IV-B. Similarly, we compute 68% confidence interval below and above mean for the lower bound and measurement success probability of our prepared GHZ state.

1) *Overall Result:* Figure 6 shows the bounds for GHZ state  $|G_N\rangle$  where  $N = 2$  to  $20$ . The GHZ states are sorted left to right according to CNOT gate counts in untranspiled GHZ circuits. The left plot shows bounds for logarithmic depth GHZ state circuits, while the right plot shows bounds for the linear depth GHZ circuits. Both plots show lower bound on quantum fidelity and measurement success probability along with 68% confidence interval below and above the mean of the distribution. For both log and linear depth circuits, the lower bound on fidelity decreases almost linearly, albeit few variations with increasing CNOT counts for higher  $N$ . The gap between lower bound and measured success probability starts to increase with increasing CNOT count. The linear circuit shows faster drop for higher GHZ states than log depth circuit which is expected as logarithmic depth circuits require less time steps for circuit execution. In both plot, we observe few irregular ups and downs in the lower bound estimation that could be because of the statistical noise. The gap between lower bound and confidence interval region stays almost close in all GHZ states. Our investigation find that expectation  $\mathcal{S}_{G_s}$  (defined as product of pauli  $X$  operations on each qubit) starts to drop from  $|G_{11}\rangle$  and becomes more significant from  $|G_{17}\rangle$ . There are two flat decrease from linear depth GHZ state  $|G_{17}\rangle$  to  $|G_{18}\rangle$  and  $|G_{19}\rangle$  to  $|G_{20}\rangle$  which could be caused by the qubit rearrangement in Quantinuum H1-1 device.

2) *Number of Shots::* To see the effect of the number of shots on quantum fidelity of GHZ states, we execute the GHZ states  $|G_N\rangle$  where  $2 \leq N \leq 20$  for 200 shots in Quantinuum H1-1 quantum device. We use 200 number of shots for all GHZ states. We estimate the cumulative lower bound distribution on quantum fidelity  $\langle G_N | \rho | G_N \rangle$  from initial to up to  $i^{th}$  shot where  $i = 2$  to 200.

Figure 7 shows the estimations of bounds on quantum fidelity  $\langle G_N | \rho | G_N \rangle$  for GHZ states on Quantinuum H1-1 quantum processor. The upper two plots (left and right) show logarithmic depth  $|G_{10}\rangle$ ,  $|G_{15}\rangle$  &  $|G_{20}\rangle$  states and the bottom

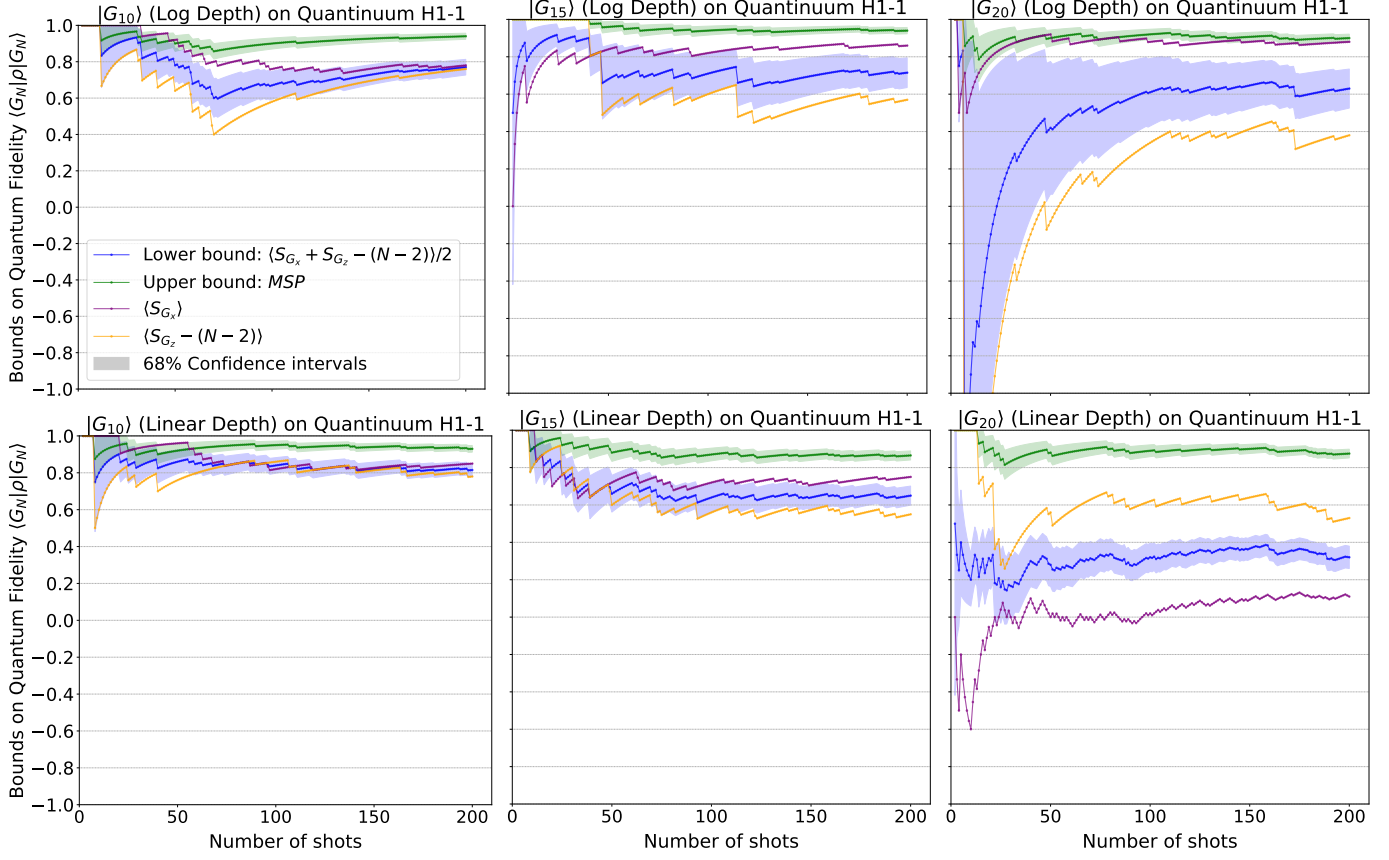


Fig. 7. Evolving bounds on quantum fidelity  $\langle G_N | \rho | G_N \rangle$  for GHZ States (left)  $|G_{10}\rangle$ , (center)  $|G_{15}\rangle$  & (right)  $|G_{20}\rangle$  on Quantinuum H1-1 over 200 shots. (top row) Plots show bounds for logarithmic depth GHZ state preparation circuits; (bottom row) plots show bounds for linear depth GHZ state preparation. Each plot shows the cumulative progress of lower bound estimation including confidence intervals. All GHZ experiments were run back to back in batch mode.

two plots (left and right) show linear depth  $|G_{10}\rangle$ ,  $|G_{15}\rangle$  &  $|G_{20}\rangle$  states. Each plot shows lower bound estimation, measured success probability and expectations of Pauli  $X$  &  $Z$  measurements for GHZ state  $|G_N\rangle$  preparation. The plots also include 68% confidence interval region below and above the mean of lower bound and measured success probability. In each plot, the cumulative measurements starts with a lot of fluctuations that becomes balanced with increasing number of shots. We observe that all the measurements are more steady in  $|G_{10}\rangle$  plot for both linear and logarithmic depth circuits than  $|G_{15}\rangle$  and  $|G_{20}\rangle$  plots. We find that the expectation  $S_{G_8}$  (purple line) drops significantly for  $|G_{20}\rangle$ . It could be possible that larger GHZ states require more shots to become stable. Additionally we observe that the confidence interval region for log depth  $|G_{20}\rangle$  circuit is less stable than linear depth circuit.

Besides, the upper bound measured success probability stays almost stable in both linear and log depth circuits.

## V. FIDELITY LOWER BOUNDS FOR APPROXIMATE DICKE STATES

Section III-C shows the linear relationship between Dicke state fidelities with increasing number of qubits ( $N$ ). For higher  $N$ , direct fidelity computation becomes exponentially

expensive in terms of time and resource. Also the lower bound estimation becomes infeasible because of the statistical noise in the system. As alternative, preparing an “approximate” Dicke state might be another option that yields Dicke states with weaker theoretical fidelities but less noise.

### A. State Preparation

We prepare two versions of “Approximate Dicke states” with (polynomially) vanishing fidelity to an actual Dicke state  $|D_K^N\rangle$ : Product states  $|PS_K^N\rangle$  for small  $K$  and Even/Odd Hamming weight states  $|E_N\rangle$ ,  $|O_n\rangle$  for large  $K$  with even/odd parity, respectively. These are defined as:

$$\begin{aligned}
 |PS_K^N\rangle &:= \left( \sqrt{1 - K/N} |0\rangle + \sqrt{K/N} |1\rangle \right)^{\otimes N} \\
 &= \sum_{i=0}^N \sqrt{\binom{N}{i} \left(\frac{K}{N}\right)^i \left(\frac{N-K}{N}\right)^{N-i}} |D_i^N\rangle \\
 |E_N\rangle &:= \sum_{x \in \{0,1\}^N, \text{wt}(x) \equiv 0 \pmod{2}} |x\rangle \\
 &= \sum_{i=0}^{\lfloor N/2 \rfloor} \sqrt{\binom{N}{2i} / 2^{n-1}} |D_{2i}^N\rangle \\
 |O_N\rangle &:= \sum_{x \in \{0,1\}^N, \text{wt}(x) \equiv 1 \pmod{2}} |x\rangle \\
 &= \sum_{i=1}^{\lfloor N/2 \rfloor} \sqrt{\binom{N}{2i-1} / 2^{n-1}} |D_{2i-1}^N\rangle
 \end{aligned}$$

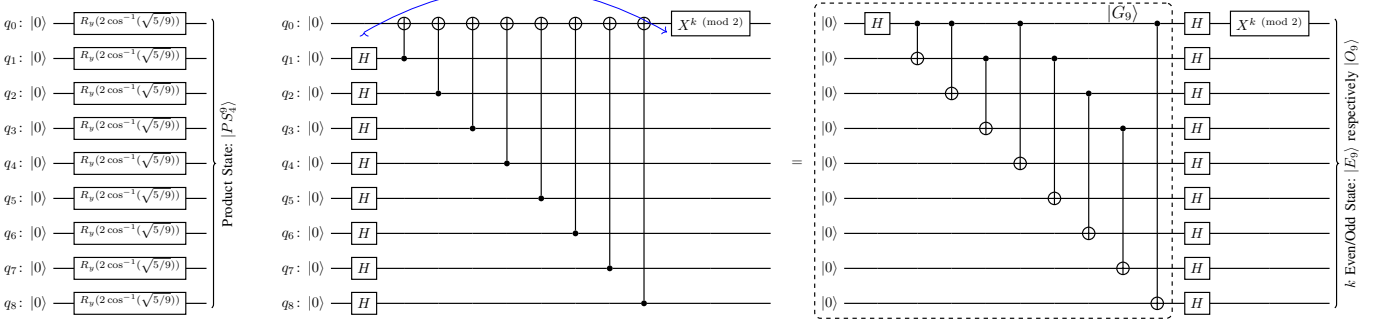


Fig. 8. Preparations of Approximate Dicke States,  $N = 9$ : (left) Product state  $|PS_4^9\rangle = (\sqrt{\frac{5}{9}}|0\rangle + \sqrt{\frac{4}{9}}|1\rangle)^{\otimes 9}$ , using parallel  $R_y(2\cos^{-1}(\sqrt{5/9}))$  rotations. (center) Schematic circuit for Even and Odd Hamming weight state preparation for  $K$  even or odd, respectively. The circuit adds the Hamming weight parity of a  $|+8\rangle$  state into the first qubit  $q_0$ . Moving a column of  $H$ -gates to the right (blue arrow) swaps controls and targets of the CNOT gates. This leads to (right) a logarithmic-depth  $|G_9\rangle$ -based state preparation circuit for Even/Odd Hamming weight states  $|E_9\rangle$ ,  $|O_9\rangle$ , depending on the parity of  $K$ .

Theoretical product state from [5] is a probabilistic approach of preparing  $N$ -qubit symmetric product state  $(\sqrt{1 - K/N}|0\rangle + \sqrt{K/N}|1\rangle)^{\otimes N}$ . The state is prepared by adding rotation  $R_y(2w\cos^{-1}(\sqrt{(n-k)/n}))$  on each qubit. We then measure them in  $X$ ,  $Y$ , and  $Z$  basis. This yields approximate Dicke state with success probability  $\binom{N}{K}(\frac{K}{N})^K(1 - \frac{K}{N})^{(N-K)}$ . To find approximate Dicke state fidelities, we generate Product state  $|PS_K^N\rangle$  for  $N = 2$  to 10 qubits and  $K = 1$  to  $N/2$ .

Another way of generating approximate Dicke states could be by preparing  $N$ -qubit odd or even hamming weight states based on the GHZ circuits discussed in Section IV-A. Even hamming weight  $N$ -qubit states are close to Dicke states  $|D_K^N\rangle$  with  $K$  even and  $N$ -qubit odd hamming weight states give approximate Dicke state  $|D_K^N\rangle$  with  $K$  odd. Odd/Even hamming weight states provide Dicke state fidelities of  $\binom{N}{K}/2^{N-1}$ .  $N$ -qubit even states are constructed by adding  $H^{\otimes N}$  at the end of  $N$ -qubit logarithmic depth GHZ circuits. For  $N$ -qubit odd states, we just flip one qubit of the even hamming state. For example, 3-qubit even hamming weight state  $\sqrt{1/4}(|000\rangle + |011\rangle + |101\rangle + |110\rangle)$  are generated from 3-qubit GHZ states  $\sqrt{1/2}(|000\rangle + |111\rangle)$ . If the first qubit is flipped from 3-qubit even hamming weight state, we get odd hamming weight state  $\sqrt{1/4}(|001\rangle + |010\rangle + |100\rangle + |111\rangle)$ . We get a closer Dicke state with higher fidelity when hamming weight is higher as Dicke state  $|D_K^N\rangle$  has  $\binom{N}{K}$  states and odd/even hamming weight states has  $2^{N-1}$  states. When  $N$  is higher but  $K$  is low, this approximate Dicke state has more non-Dicke states than Dicke states, therefore, the fidelity gets lower. Thus, we expect higher fidelity with increasing  $K/N$ . We construct odd hamming weight states  $|O_N\rangle$  for  $N = 2$  to 10 qubits and even hamming weight states  $|E_N\rangle$  for  $N = 4$  to 10 qubits.

### B. Lower bounds for Fidelity Estimation

For  $N$ -qubit product state  $|PS_K^N\rangle$ , we compute lower bound estimations on Dicke state fidelity using the expressions from Section III-B. Similarly, we estimate Dicke state fidelity for odd and even hamming weight states. When  $K$  is odd, we estimate a lower bound on fidelity for odd hamming weight

state  $|O_N\rangle$ , and for even  $K$ , we compute a lower bound on fidelity for even hamming weight state  $|E_N\rangle$ .

### C. Experimental Result

We prepare untranspiled circuits for product states  $|PS_K^N\rangle$  where  $1 \leq 2K \leq N \leq 10$ , odd hamming weight states  $|O_N\rangle$  where  $2 \leq N \leq 10$  and even hamming weight states  $|E_N\rangle$  where  $4 \leq N \leq 10$ . Figure 8 shows preparation of approximate Dicke States for  $N = 9$ . We execute the circuits in Quantinuum H1-1 quantum processor to get  $X$ ,  $Y$ , and  $Z$  basis measurements similar to Dicke state circuits in Section III-C. We then compute experimental lower bound on Dicke state fidelities for product states and odd/even states. Figure 9 shows the experimental bounds on Dicke state fidelities using the approximate Dicke state circuits. The plot shows bounds on quantum fidelity  $\langle D_K^N | \rho | D_K^N \rangle$  for  $N = 2$  to  $N = 10$  qubits. In each plot, the  $X$  axis shows values for  $K/N$  and the  $Y$  axis shows bounds on fidelity. Each plot contains two lines showing theoretical fidelity of odd/even state and product state preparation with Dicke state. In each plot, the bounds (theoretical and experimental) increase for odd/even state with higher  $K/N$  but decreases for product states. Experimental lower bounds are also shown for odd/even state, product state, and Dicke state (from Section III-C) preparation. We find that the experimental lower bounds of the product state closely follow theoretical fidelities in all the plots ( $N = 2$  to 10). However, the experimental lower bounds of odd/even states are not close but follow theoretical fidelities. We also observe that the approximate lower bounds of product state and odd/even state are getting close to Dicke state lower bounds with higher  $N$  and for  $N = 10$  and  $K = 5$ , the odd/even state lower bounds match with Dicke state lower bound estimations. Thus, we can get a good approximation of lower bounds on Dicke state fidelities from just preparing those approximate states for higher Dicke states.

## VI. METHODOLOGY

Our access to the Quantinuum backends was granted through OLCF program of Oak Ridge National Laboratory. In this work, we ran the experiments on both hardware and

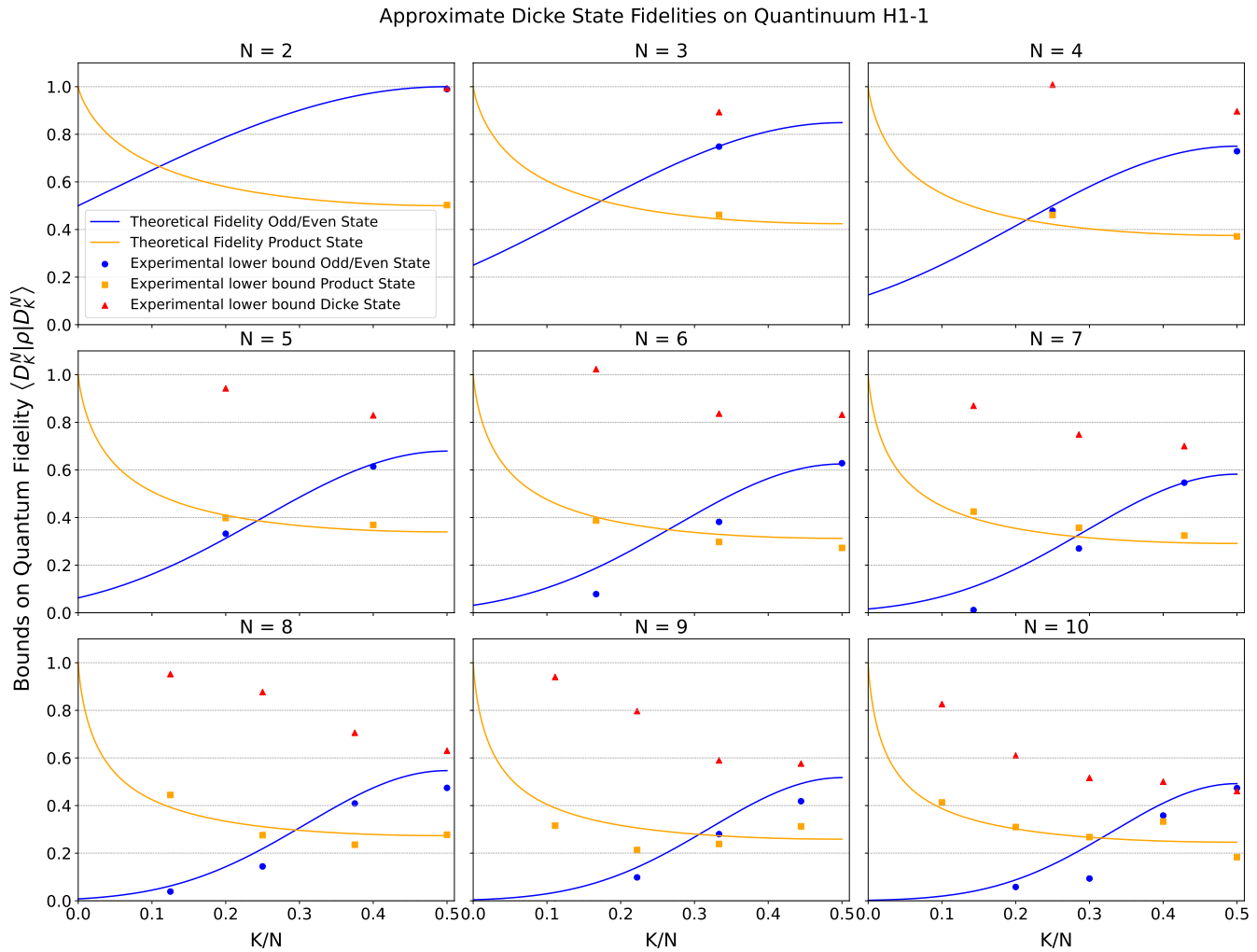


Fig. 9. Approximate Dicke State (Product State and Odd/Even State) fidelities with Dicke State and their Lower Bound estimation for  $N = 2$  to  $10$ . Each plot shows theoretical & experimental fidelity for approximate Dicke states along with the lower bound estimations of the prepared Dicke states. Data points are plotted along the  $x$ -axes according to the ratio  $K/N$ ; theoretical fidelities are plotted as continuous lines to visualize the trend when going to higher  $N$ .

emulator devices of Quantinuum H-systems using the Quantinuum Python API. Running jobs on Quantinuum backend costs requires H-System Quantum Credits (HQC) that is linear with both number of shots per circuit and number of CNOTs in the circuit. In general, the total cost scales with the product of number of shots and CNOT counts. Our initial goal was to determine number of experiments and number of shots for different state preparation permissible within the HQCs allocated to us. As the Quantinuum machine's are available throughout a calendar month and HQCs are allocated monthly, we target to complete experiments over the duration of a couple of months with available hardware credits. First we ran the experiments on Quantinuum H1-2E emulator to get an estimation the confidence interval sizes we can expect from the quantum hardware. To see the effect of the number of circuit execution, we compute the cumulative bounds for fidelity and measured success probability. Similarly, we compute two-sided 68% confidence interval below and above the mean of

the distribution to check the stability of the bounds with the increasing number of shots. Analyzing the results of emulator experiments, we get an approximation on the meaningful number of different experiments than can be performed on quantum hardware for various states. We limit Dicke state preparation upto  $N = 10$  as Dicke States above  $N = 11$  becomes too costly. For GHZ states, we went upto  $N = 20$  as we ran the experiment on 20-qubit H1-1 device. Additionally, we observe roughly equal confidence interval widths for the bounds across the experiments. Next, we execute the experiments of different state preparation on Quantinuum hardware backends depending on their availability. Dicke state circuits were executed in the 12 qubit H1-2 quantum processor while GHZ state and approximate Dicke state circuits were executed in the 20 qubit H1-1 quantum processor. For all experiments, we directly submit the QASM [6] code using the Python API. To execute the circuits in the same time span, we submit the jobs in batch mode where we only have to wait the queue

time once. However, Quantinuum queue only allows 500 HQC execution in a single batch. Thus, we had to execute sub-experiments over a couple of months. Dicke states experiments were run in this way,  $|D_1^2\rangle$  to  $|D_2^7\rangle$  on May 24th,  $|D_1^8\rangle$  to  $|D_2^9\rangle$  on June 6th,  $|D_3^9\rangle$  to  $|D_3^{10}\rangle$  on June 10th,  $|D_4^{10}\rangle$  on June 17th and  $|D_5^{10}\rangle$  on July 25th of 2022. Both logarithmic depth and linear depth GHZ circuits were executed on August 19th of 2022. Approximate Dicke states (odd/even states and product states) were executed on July 12th of 2022.

## VII. CONCLUSION

We have demonstrated good fidelity values for highly entangled quantum states such as Dicke and GHZ states, prepared on Quantinuum H1 ion trap systems. Since direct fidelity estimation through full state tomography does not scale, we have applied and improved existing lower bound techniques, achieving reasonable estimations on NISQ devices for the first time in 15 years.

## REFERENCES

- [1] Qiskit: An open-source framework for quantum computing, 2021. URL: <https://qiskit.org/>, doi:10.5281/zenodo.2573505.
- [2] Shaminuj Aktar, Andreas Bärtschi, Abdel-Hameed A Badawy, and Stephan Eidenbenz. A Divide-and-Conquer Approach to Dicke State Preparation. *IEEE Transactions on Quantum Engineering*, 3:1–16, 2022. arXiv:2112.12435, doi:10.1109/TQE.2022.3174547.
- [3] Andreas Bärtschi and Stephan Eidenbenz. Deterministic Preparation of Dicke States. In *22nd International Symposium on Fundamentals of Computation Theory, FCT’19*, pages 126–139, 2019. arXiv:1904.07358, doi:10.1007/978-3-030-25027-0\_9.
- [4] Andreas Bärtschi and Stephan Eidenbenz. Short-Depth Circuits for Dicke State Preparation. In *IEEE International Conference on Quantum Computing & Engineering QCE’22*, 2022. To appear. arXiv:2207.09998.
- [5] Andrew M Childs, Edward Farhi, Jeffrey Goldstone, and Sam Gutmann. Finding cliques by quantum adiabatic evolution. *Quantum Information & Computation*, 2000. arXiv:quant-ph/0012104, doi:10.5555/2011430.2011431.
- [6] Andrew W Cross, Lev S Bishop, John A Smolin, and Jay M Gambetta. Open quantum assembly language. *arXiv preprint*, 2017. arXiv:1707.03429.
- [7] Cruz, Diogo and Fournier, Romain and Gremion, Fabien and Jeannerot, Alix and Komagata, Kenichi and Tosic, Tara and Thiesbrummel, Jarla and Chan, Chun Lam and Macris, Nicolas and Dupertuis, Marc-André and Javerzac-Galy, Clément. Efficient Quantum Algorithms for GHZ and W States, and Implementation on the IBM Quantum Computer. *Advanced Quantum Technologies*, 2(5-6):1900015, 2019. arXiv:1807.05572, doi:10.1002/qute.201900015.
- [8] Andreas Elben, Steven T Flammia, Hsin-Yuan Huang, Richard Kueng, John Preskill, Benoît Vermersch, and Peter Zoller. The randomized measurement toolbox. *arXiv preprint*, 2022. arXiv:2203.11374.
- [9] Steven T Flammia and Yi-Kai Liu. Direct fidelity estimation from few Pauli measurements. *Physical Review Letters*, 106(23):230501, 2011. arXiv:1104.4695, doi:10.1103/PhysRevLett.106.230501.
- [10] Daniel Gottesman. *Stabilizer codes and quantum error correction*. Caltech Ph. D. PhD thesis, Thesis, eprint, 1997. arXiv:quant-ph/9705052.
- [11] Otfried Gühne, Chao-Yang Lu, Wei-Bo Gao, and Jian-Wei Pan. Toolbox for entanglement detection and fidelity estimation. *Physical Review A*, 76(3):030305, 2007. arXiv:0706.2432, doi:10.1103/PhysRevA.76.030305.
- [12] Xinhe Jiang, Kun Wang, Kaiyi Qian, Zhaozhong Chen, Zhiyu Chen, Liangliang Lu, Lijun Xia, Fangmin Song, Shining Zhu, and Xiaosong Ma. Towards the standardization of quantum state verification using optimal strategies. *npj Quantum Information*, 6(1):1–8, 2020. arXiv:2002.00640, doi:10.1038/s41534-020-00317-7.
- [13] Richard Jozsa. Fidelity for mixed quantum states. *Journal of Modern Optics*, 41(12):2315–2323, 1994.
- [14] Zihao Li, Yun-Guang Han, and Huangjun Zhu. Efficient verification of bipartite pure states. *Physical Review A*, 100(3):032316, 2019. arXiv:1901.09783, doi:10.1103/PhysRevA.100.032316.
- [15] Zihao Li, Yun-Guang Han, and Huangjun Zhu. Optimal verification of greenberger-horne-zeilinger states. *Physical Review Applied*, 13(5):054002, 2020. arXiv:1909.08979, doi:10.1103/PhysRevApplied.13.054002.
- [16] Ye-Chao Liu, Xiao-Dong Yu, Jiangwei Shang, Huangjun Zhu, and Xiangdong Zhang. Efficient verification of Dicke states. *Physical Review Applied*, 12(4):044020, 2019. arXiv:1904.01979, doi:10.1103/PhysRevApplied.12.044020.
- [17] Chandra Sekhar Mukherjee, Subhamoy Maitra, Vineet Gaurav, and Dibyendu Roy. Preparing Dicke States on a Quantum Computer. *IEEE Transactions on Quantum Engineering*, 1:1–17, 2020. doi:10.1109/TQE.2020.3041479.
- [18] Michael A. Nielsen and Isaac L. Chuang. *Quantum Computation and Quantum Information*. Cambridge University Press, 2000.
- [19] Sam Pallister, Noah Linden, and Ashley Montanaro. Optimal verification of entangled states with local measurements. *Physical Review Letters*, 120(17):170502, 2018. arXiv:1709.03353, doi:10.1103/PhysRevLett.120.170502.
- [20] Rolando D Somma, John Chiaverini, and Dana J Berkeland. Lower bounds for the fidelity of entangled-state preparation. *Physical Review A*, 74(5):052302, 2006. arXiv:quant-ph/0606023, doi:10.1103/PhysRevA.74.052302.
- [21] Yuuki Tokunaga, Takashi Yamamoto, Masato Koashi, and Nobuyuki Imoto. Fidelity estimation and entanglement verification for experimentally produced four-qubit cluster states. *Physical Review A*, 74(2):020301, 2006. doi:10.1103/PhysRevA.74.020301.
- [22] Kun Wang and Masahito Hayashi. Optimal verification of two-qubit pure states. *Physical Review A*, 100(3):032315, 2019. arXiv:1901.09467, doi:10.1103/PhysRevA.100.032315.
- [23] Xiao-Dong Yu, Jiangwei Shang, and Otfried Gühne. Optimal verification of general bipartite pure states. *npj Quantum Information*, 5(1):1–5, 2019. arXiv:1901.09856, doi:10.1038/s41534-019-0226-z.
- [24] Wen-Hao Zhang, Chao Zhang, Zhe Chen, Xing-Xiang Peng, Xiao-Ye Xu, Peng Yin, Shang Yu, Xiang-Jun Ye, Yong-Jian Han, Jin-Shi Xu, et al. Experimental optimal verification of entangled states using local measurements. *Physical Review Letters*, 125(3):030506, 2020. arXiv:1905.12175, doi:10.1103/PhysRevLett.125.030506.
- [25] Xiaoqian Zhang, Maolin Luo, Zhaodi Wen, Qin Feng, Shengshi Pang, Weiqi Luo, and Xiaoqi Zhou. Direct fidelity estimation of quantum states using machine learning. *Physical Review Letters*, 127(13):130503, 2021. arXiv:2102.02369, doi:10.1103/PhysRevLett.127.130503.
- [26] Huangjun Zhu and Masahito Hayashi. Efficient verification of hypergraph states. *Physical Review Applied*, 12(5):054047, 2019. arXiv:1806.05565, doi:10.1103/PhysRevApplied.12.054047.
- [27] Huangjun Zhu and Masahito Hayashi. Efficient verification of pure quantum states in the adversarial scenario. *Physical Review Letters*, 123(26):260504, 2019. arXiv:1909.01900, doi:10.1103/PhysRevLett.123.260504.
- [28] Huangjun Zhu and Masahito Hayashi. General framework for verifying pure quantum states in the adversarial scenario. *Physical Review A*, 100(6):062335, 2019. arXiv:1909.01943, doi:10.1103/PhysRevA.100.062335.
- [29] Huangjun Zhu and Masahito Hayashi. Optimal verification and fidelity estimation of maximally entangled states. *Physical Review A*, 99(5):052346, 2019. arXiv:1901.09772, doi:10.1103/PhysRevA.99.052346.